

TTP99-30

# Deep-inelastic Electron-Photon Scattering at High $Q^2$ : Neutral and Charged Current Reactions

A. Gehrmann–De Ridder <sup>a</sup>

<sup>a</sup> Institut für Theoretische Teilchenphysik, Universität Karlsruhe, D-76128 Karlsruhe, Germany and Deutsches Elektronen-Synchrotron DESY, D-22603 Hamburg, Germany.

We present the results of a calculation of deep inelastic electron-photon scattering at a linear collider for very high virtuality of the intermediate gauge boson up to NLO in perturbative QCD. The real photon is produced unpolarized via the Compton back scattering of laser light of the incoming beam. For  $Q^2$  values close to the masses squared of the Z and W gauge bosons, the deep inelastic electron-photon scattering process receives important contributions not only from virtual photon exchange but also from the exchange of a Z-boson and a W-boson. We find that the total cross section for center of mass energies above 500GeV is at least of  $\mathcal{O}(pb)$  and has an important charged current contribution.

## 1. Introduction

Processes induced by initial state photons provide us with an interesting testing ground for QCD. As a photon can interacts directly through a pointlike coupling with quarks or through its parton content like a hadron it has a twofold nature. Its point-like interaction gives rise to perturbatively calculable short-distance contributions [1] while its hadron-like or resolved part cannot be described with perturbative methods. It is described in terms of the parton distribution functions inside the photon. These parton distributions obey a perturbative evolution equation with a non-perturbative boundary condition usually parameterized in the form of an initial distribution at some low starting scale  $\mu_0$ . The pointlike and resolved processes contribute to the various real structure functions entering the cross section for  $e^+e^- \rightarrow e^- + \gamma \rightarrow l + X$ , the object of this study.

## 2. The photon spectrum

The process of Compton backscattering of laser beams off highly energetic electrons/positrons offers an efficient mechanism to transfer a large fraction of the lepton energy to the photon which structure can be investigated in deep inelastic electron-photon scattering.

The differential Compton cross section for the process  $e^\pm + \gamma \rightarrow e^\pm + \gamma'$ , where the polarization of the final state photon  $\gamma'$  is not observed takes the following form [2,3],

$$\frac{d\sigma}{dy_\gamma} = \frac{\pi\alpha^2}{x_0 m_e^2} \left\{ \frac{1}{1-y} + (1-y) - 4r(1-r) + P_e P_\gamma x_0 r (1-2r)(2-y) \right\}. \quad (1)$$

The energy transferred from the electron to the backscattered photon is denoted by  $y_\gamma$ .  $P_e, P_\gamma$  are the helicities of the incoming lepton and laser photon with  $-1 \leq P_e, P_\gamma \leq 1$ . In the above formula, the ratio  $r = y/[(1-y)x_0]$  while the fractional energy of the final state photon  $y_\gamma$  is bounded by  $y_\gamma \leq \frac{x_0}{1+x_0}$ . The parameter  $x_0$  is defined as  $\frac{4Ew_0}{m_e^2}$  where  $E$  and  $w_0$  are the energies of the incoming electron and photon. By tuning the energy of the incoming photon, the parameter  $x_0$  can be chosen close to 4.83, just below the threshold for production of  $e^+e^-$  pairs from the collision of laser and final state photons. To give an order of magnitude, for an energy of the incoming lepton of 250 GeV, the laser energy is of the order of 1 eV.

It is worth noting that the photon luminosity for backscattered photons is of the same order as the initial electron luminosity. It is therefore enhanced compared to the photon luminosity ob-

tained for photon produced by bremsstrahlung off the lepton which is of  $\mathcal{O}(\alpha)$ . Furthermore, by choosing the helicities of laser and electron beams to be opposite, the photon spectrum is peaked at high energies. In this region, about 80% of the energy of the electron/positron beam can be transferred to the backscattered photon. In the following we shall give our predictions for the most advantageous photon spectrum and will therefore consider the backscattered photon obtained for opposite polarizations of electron and laser photon, with  $x_0 = 4.83$ . Our results will be obtained for the cross section  $e^+e^- \rightarrow l+X$  which is related to the cross section for  $e^-\gamma \rightarrow l+X$  as follows,

$$d\sigma_{e^+e^- \rightarrow l+X} = \int dy_\gamma \frac{1}{\sigma_c} \frac{d\sigma_c}{dy_\gamma} d\sigma_{e^+\gamma \rightarrow l+X}. \quad (2)$$

### 3. Deep-Inelastic Electron-Photon scattering

At momentum transfer squared  $Q^2$  close to the Z and W masses squared, the deep inelastic cross section for  $e + \gamma \rightarrow l + X$  becomes sensitive to contributions from these exchanges [4]. Neutral current deep inelastic events are characterized by the exchange of a photon or a Z boson, and have an electron and a jet (or jets) in the final state. Charged current events arise via the exchange of a W-boson and contain an undetected neutrino and a jet (or jets) in the final state. The presence of an neutrino is as usual detected as missing transverse momentum. Having these signatures, those processes constitute potential background sources for searches for new physics at the future  $e^+e^-$  linear collider. To give a prediction for the size of these contributions is precisely the aim of this study.

#### 3.1. Kinematics

The neutral current differential cross section is parameterized by the  $x$  and  $Q^2$  dependent structure functions  $F_2^{\gamma,NC}$  and  $F_L^{\gamma,NC}$ ,

$$\frac{d^2\sigma^{NC}(e + \gamma \rightarrow e + X)}{dx dQ^2} = \frac{2\pi\alpha^2}{xQ^4} \left[ (1 + (1 - y)^2)F_2^{\gamma,NC} - y^2F_L^{\gamma,NC} \right] \quad (3)$$

while in the charged current differential cross section enter the  $x$  and  $Q^2$  dependent structure functions  $F_2^{\gamma,CC}$ ,  $F_L^{\gamma,CC}$  and  $F_3^{\gamma,CC}$  multiplied by weak propagator and coupling factors as follows

$$\begin{aligned} \frac{d^2\sigma^{CC}(e^\pm + \gamma \rightarrow \bar{\nu}^\pm + X)}{dx dQ^2} &= \\ \frac{1}{4} \frac{\pi\alpha^2}{xQ^4} &\frac{Q^4}{[Q^2 + M_W^2]^2} \frac{(1 \pm P)}{\sin^4 \Theta_w} \\ &\left[ (1 + (1 - y)^2)F_2^{\gamma,CC} \right. \\ &\left. \mp (1 - (1 - y)^2)x F_3^{\gamma,CC} - y^2 F_L^{\gamma,CC} \right]. \end{aligned} \quad (4)$$

$M_W$  and  $\Theta_W$  are the W-mass and the weak Weinberg angle.  $P$  denotes the degree of left-handed longitudinal polarization ( $P = -1$  for left-handed electrons,  $P = 1$  for right-handed electrons).

The kinematics of these neutral and charged current reactions is described by the Bjorken variables  $x$  and  $y$ . Those can be expressed in terms of the four-momentum transfer,  $Q^2$ , the hadronic energy  $W$ , the lepton energies and scattering angles. Indeed we have,

$$\begin{aligned} x &= \frac{Q^2}{2q \cdot p_\gamma} = \frac{Q^2}{Q^2 + W^2} \\ y &= \frac{q \cdot p_\gamma}{k \cdot p_\gamma} = 1 - \frac{E}{E'} \cos^2(\Theta/2). \end{aligned} \quad (5)$$

The initial state photon is real and on-shell and the lepton masses can be set to zero.

Experimentally, one needs to constrain the lepton scattering angle  $\Theta_e$  to be larger than some minimum angle  $\Theta_{min}$ . Equivalently, one can also require,

$$\begin{aligned} Q^2 &> \frac{4E^2(1 - c_o)x s_{e\gamma}}{x s_{e\gamma}(1 + c_o) + 4E^2(1 - c_o)} \\ Q^2 &> Q^2(x, s_{e\gamma}, c_o) \end{aligned} \quad (6)$$

with  $c_o = \cos \Theta_{min}$  and  $s_{e\gamma}$  the electron-photon center-of-mass energy squared. This constraint on the 4-momentum transfer  $Q^2$  is shown as a function of  $x$  in Fig. 1 for  $\sqrt{s}_{e\gamma} = 500$  GeV and for  $\Theta_{min} = 5, 10, 20$  degrees. The corresponding allowed kinematical regions are then situated between  $Q^2 = Q^2(x, s_{e\gamma}, c_o)$  and  $Q^2 = x s_{e\gamma}$  (corresponding to  $y = 1$ ).

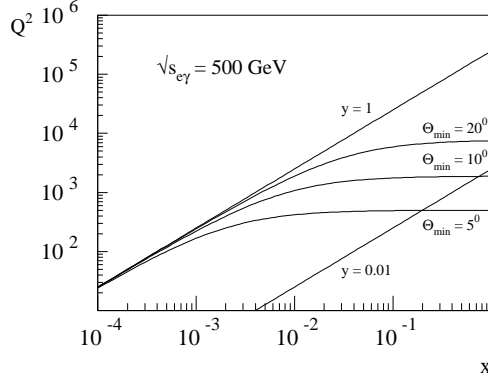


Figure 1. The kinematical region corresponding to  $\Theta_{min} = 5, 10, 20$  degrees, for  $\sqrt{s}_{e\gamma} = 500$  GeV.

In this study, we will choose to present our results for fixed minimum values of  $Q^2$ . For illustrative purpose, in Table 1 we present the choices of  $Q_{min}^2$  corresponding to different electron-photon center of mass energy and  $\Theta_{min}$  values.

### 3.2. Neutral and charged current structure functions

The neutral and charged current structure functions appearing in eqs. (3) and (4) depend on the Bjorken variable  $x$  and on the 4-momentum transfer  $Q^2$ ; in our study,  $x$  typically lies between  $10^{-3}$  and 0.8, while  $Q^2$  takes values close to the masses squared of the Z and W bosons.  $Q^2$  being the only large scale in this study, the structure functions follow a perturbative expansion in  $\alpha_s \log(Q^2)$ , an expansion in the leading and next-to-leading logarithmic terms. Furthermore, neutral and charged structure functions have different components coming from the various flavour-dependent parton distributions building them up.

The neutral current structure functions  $F_2^{\gamma,NC}$  and  $F_L^{\gamma,NC}$  receive contributions from 6 quark flavours. Except for the top quark, the masses of the 5 lightest quark are negligible compared to the scale  $Q^2$ . These flavours can be treated as massless and their contributions to  $F_2^{\gamma,NC}$  and  $F_L^{\gamma,NC}$  are connected to the massless parton distributions in the photon. Those distributions are

Table 1  
The different  $Q_{min}^2$  values, see text

$\sqrt{s}_{e\gamma}$ (GeV)	500	1000	2000	
$Q_{min}^2$ (GeV $^2$ )	$10^4$	$5 \cdot 10^4$	$10^5$	$20^\circ$
	$10^3$	$5 \cdot 10^3$	$5 \cdot 10^4$	$10^\circ$
	$5 \cdot 10^2$	$5 \cdot 10^3$	$10^4$	$5^\circ$

solution of the all-order DGLAP evolution equations in the leading or next-to-leading logarithmic approximation where respectively only terms in  $\alpha_s^n \log^{n+1} Q^2$  or  $\alpha_s^n \log^{n+1} Q^2$  and  $\alpha_s^n \log^n Q^2$  are retained.

The different quark contributions need furthermore to be multiplied by the corresponding quark charges. As the virtual  $\gamma$  exchange is supplemented by Z-boson exchange at high virtuality  $Q^2$  the charge factor becomes,

$$e_q^2 \rightarrow \hat{e}_q^2 := \frac{1}{4} \sum_{i,j=L,R} \left[ e_q - \frac{Q^2}{Q^2 + M_Z^2} \frac{Z_i(e) Z_j(q)}{\sin^2 \Theta_w \cos^2 \Theta_w} \right]^2 \quad (7)$$

where the electroweak Z charges are given by

$$\begin{aligned} Z_L(f) &= I_{3L}(f) - e_f \sin^2 \Theta_w \\ Z_R(f) &= -e_f \sin^2 \Theta_w \end{aligned} \quad (8)$$

for the left and right-handed Z-couplings. Only the 4 lightest quark flavours contribute to the charged current structure functions through a combination of massless quark  $q(x, Q^2)$  and anti-quark  $\bar{q}(x, Q^2)$  distributions in the photon. Bottom and top contributions are here neglected as these are considerably smaller.

More explicitly, at the lowest order, for the neutral current structure functions we have,

$$F_2^{\gamma,NC} = x \sum_q \hat{e}_q^2 \{ q(x, Q^2) + \bar{q}(x, Q^2) \} \quad (9)$$

where the sum runs over the 5 lightest flavours. The top quark contribution to  $F_2^{\gamma,NC}$  is given at this order by

$$F_{2,t}^{\gamma,NC} = \frac{\alpha_s(Q^2)}{\pi} [C_g \otimes g(x)] + \frac{\alpha}{\pi} \hat{e}_q^2 C_\gamma. \quad (10)$$

$F_{2,t}^{\gamma,NC}$  is the only non-vanishing longitudinal structure function at this order.

For the scattering of an  $e^-$  with the photon, the charged current structure functions  $F_2^{\gamma,CC}$  and  $F_3^{\gamma,CC}$  at the lowest order are respectively given by,

$$\begin{aligned} F_2^{\gamma,CC} &= x [u(x, Q^2) + c(x, Q^2) \\ &\quad + \bar{d}(x, Q^2) + \bar{s}(x, Q^2)] \\ F_3^{\gamma,CC} &= [u(x, Q^2) + c(x, Q^2) \\ &\quad - \bar{d}(x, Q^2) - \bar{s}(x, Q^2)]. \end{aligned} \quad (11)$$

For  $e^+$  scattering, one has to make the following replacements:  $u(x, Q^2) + c(x, Q^2) \rightarrow \bar{u}(x, Q^2) + \bar{c}(x, Q^2)$  and  $\bar{d}(x, Q^2) + \bar{s}(x, Q^2) \rightarrow d(x, Q^2) + s(x, Q^2)$ . The CKM matrix is approximated by the unity matrix, flavour mixing effects can here be neglected.

At the next-to-leading order, corrections proportional to  $\alpha_s \log(Q^2)$  have to be included in all the above leading-order expressions. To the terms proportional to the parton distributions themselves, terms involving convolution of these with quark ( $C_q$ ) and gluon ( $C_g$ ) coefficient functions have to be taken into account. For example, for the light flavours,  $F_2^{\gamma,NC}$  given at leading order in eq.(9) becomes in the  $\overline{\text{MS}}$  scheme at the next-to-leading order

$$\begin{aligned} F_2^{\gamma,NC} &= x \sum_q \hat{e}_q^2 \{q(x, Q^2) + \bar{q}(x, Q^2)\} \\ &\quad + \frac{\alpha_s(Q^2)}{2\pi} \left[ C_q \otimes \{q(x, Q^2) + \bar{q}(x, Q^2)\} \right. \\ &\quad \left. + C_g \otimes g(x, Q^2) \right] + \frac{\alpha}{\pi} C_{\gamma,2}. \end{aligned} \quad (12)$$

At this order, we use the beyond-leading-logarithmic (BLL) GRV [5] massless parton distributions  $q(x, Q^2)$  and  $g(x, Q^2)$ . These are given in the  $DIS_\gamma$  factorization scheme, defined by,

$$q(x, Q^2)_{DIS_\gamma} = q(x, Q^2)_{\overline{\text{MS}}} + \frac{\alpha}{2\pi} C_{\gamma,2}. \quad (13)$$

As a consequence, in this  $DIS_\gamma$  factorization scheme the direct term  $C_{\gamma,2}$  is absent from the expression of  $F_2^{\gamma,NC}$ . The gluon distribution  $g(x, Q^2)$  remains unaffected by the change of factorization scheme. The precise expressions of the other neutral and charged structure functions at the next-to-leading order will be given in [6].

#### 4. Results and conclusion

As mentioned before, we shall present our results for fixed values of  $Q_{min}^2$ , namely  $Q_{min}^2 = 10000 \text{ GeV}^2$  and  $Q_{min}^2 = 1000 \text{ GeV}^2$ . Since the leading and next-to-leading order results are found to be very close to each other, all results will be given at the next-to-leading order level only. The NLO corrections being at most of the percent level indicates furthermore that the obtained results are perturbatively stable.

In Figs. 2 and 3 we present the different contributions to the total NC and CC cross sections as a function of the electron-positron center of mass energy, the latter varying between  $\sqrt{s} = 200 \text{ GeV}$  and  $\sqrt{s} = 2000 \text{ GeV}$  for virtualities of the intermediate gauge boson equal to  $10000 \text{ GeV}^2$  and  $1000 \text{ GeV}^2$  respectively.

The cross sections being inversely proportional to  $Q^4$ , their value is dominated by the smallest  $Q^2$  values. As can be seen in these figures, for  $Q_{min}^2 = 10000 \text{ GeV}^2$ , the largest cross section, the total charged current cross section is of  $\mathcal{O}(pb)$  while for  $Q_{min}^2 = 1000 \text{ GeV}^2$ , the dominant neutral current cross section is about 10 times larger. For this latter choice of  $Q_{min}^2$  the charged current cross section is approximately a third of the neutral current cross section. By these high virtualities of the intermediate gauge boson, the exchange of a W-boson gives always rise to significantly high cross sections. The contribution arising from the exchange of a Z-boson is the smallest for both choices of  $Q_{min}^2$ .

The differential cross sections with respect to  $x$ , which are shown for  $\sqrt{s} = 500 \text{ GeV}$  in Figs. 4 and 5 differ not only in magnitude but also in shape. This can be understood as follows. For a given value of  $x$ , the allowed phase space regions in the  $(x, Q^2)$  plane corresponding to the two values of  $Q_{min}^2$  chosen here, differ significantly from each other. As can be seen in Fig. 1, this results in an enhanced importance of the small  $x$  region for smaller  $Q_{min}^2$ .

Finally, we also present the differential cross section with respect to  $Q^2$  for  $Q^2$  values varying between  $1000 \text{ GeV}^2$  and the electron-positron center-of-mass energy squared  $s$ , for  $\sqrt{s} = 500 \text{ GeV}$ . As can be seen in Fig. 6 the neutral

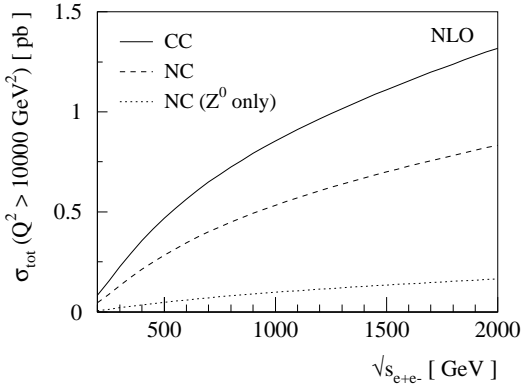


Figure 2. The total cross section as function of  $\sqrt{s}$  for  $Q_{min}^2 = 10000 \text{ GeV}^2$ .

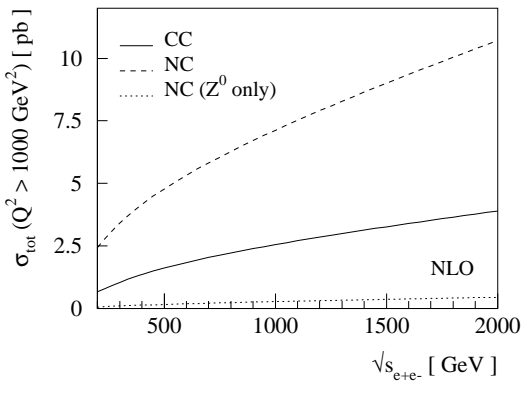


Figure 3. The total cross section as function of  $\sqrt{s}$  for  $Q_{min}^2 = 1000 \text{ GeV}^2$ .

and charged current cross sections fall off as  $Q^2$  increases. Above  $Q^2 = 10000 \text{ GeV}^2$  the CC cross section is the largest while below this value of  $Q^2$  the NC reaction induced by the exchange of an intermediate photon gives rise to the largest differential cross section with respect to  $Q^2$ .

### Acknowledgements

I wish to thank H. Spiesberger and P. Zerwas for a fruitful collaboration and A. Wagner for financial support during my stay at DESY where part of this work was carried out. Furthermore I wish to thank S. Soldner-Rembold for organizing

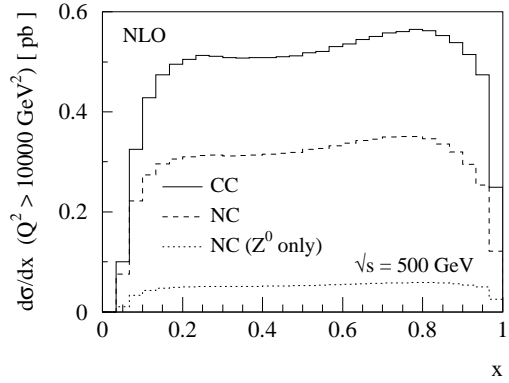


Figure 4. The differential cross section as a function of  $x$  for  $Q_{min}^2 = 10000 \text{ GeV}^2$ .

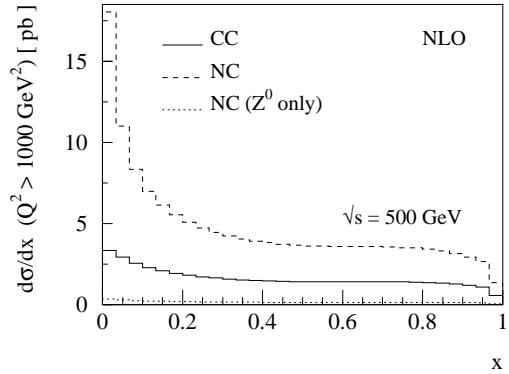


Figure 5. The differential cross section as a function of  $x$  for  $Q_{min}^2 = 1000 \text{ GeV}^2$ .

an interesting and pleasant workshop.

### REFERENCES

1. T.F. Walsh, and P. Zerwas, Phys. Lett. **B44** (1973) 195;
2. J. Kühn, E. Mirkes, J. Steegborn, Z. Phys. **C57** (1993) 615.
3. I.F. Ginzburg, G.L. Kotkin, S.L. Panfil, V.G. Serbo and V.I. Telnov, Nucl. Instr. Meth. **219** (1984) 5.
4. A. Cordier and P.M. Zerwas, Proc. "EFCA Workshop on LEP 200", Aachen 1986, CERN 87-08.

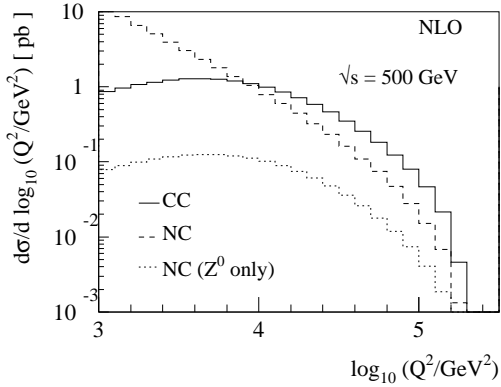


Figure 6. The differential cross section as a function of  $Q^2$ .

5. M. Glück, E. Reya and A. Vogt, Phys. Rev. **D46** (1992) 1973.
6. A. Gehrmann–De Ridder, H. Spiesberger, P.M. Zerwas, (in preparation).